Chinese Chemical Letters 34 (2023) 107503

Contents lists available at ScienceDirect

Chinese Chemical Letters

journal homepage: www.elsevier.com/locate/cclet

$NiCo_2O_4/BiOCl/Bi_{24}O_{31}Br_{10}$ ternary Z-scheme heterojunction enhance peroxymonosulfate activation under visible light: Catalyst synthesis and reaction mechanism

Tianren Li[a,b,1], Yueyu Song[a,b,1], Jingjing Jiang[a,b], Mingyu Li[a,b], Yuhan Ma[a,b], Shuangshi Dong[a,b,*]

[a] Key Laboratory of Groundwater Resources and Environment, Ministry of Education, Jilin University, Changchun 130026, China
[b] Jilin Provincial Key Laboratory of Water Resources and Environment, Jilin University, Changchun 130026, China

ARTICLE INFO

Article history:
Received 27 February 2022
Revised 22 April 2022
Accepted 10 May 2022
Available online 13 May 2022

Keywords:
Peroxymonosulfate activation
Photo-assisted Fenton-like reaction
Z-scheme heterojunction
Reaction mechanism
Reactive oxygen species

ABSTRACT

The Z-scheme heterostructure for photocatalyst can effectively prolong the lifetime of photogenerated carriers and retain a higher conduction/valence band position, promoting the synergistic coupling of photocatalysis and peroxymonosulfate (PMS) activation. In order to fully utilize the luminous energy and realize the efficient activation of PMS, this work achieved successful construction of $NiCo_2O_4/BiOCl/Bi_{24}O_{31}Br_{10}$ ternary Z-scheme heterojunction by simultaneously synthesizing BiOCl and $NiCo_2O_4$ with $NiCl_2$ and $CoCl_2$ as the precursors. The intercalated BiOCl could serve as a carrier migration ladder to further achieve the spatial separation of electron-hole pairs, so that the oxidation and reduction processes separately occurred in different regions. Compared with the reported catalysts, the as-prepared composites exhibited the enhanced removal efficiency for tetracycline hydrochloride (TCH) in the visible light/PMS system, with a degradation efficiency of 85.30% in 2 min, and possessed good stability. Z-scheme heterojunction was shown to be beneficial for maximizing the superiority of photo-assisted Fenton-like reaction system. The experimental and characterization results confirmed that both non-radicals ($^1O_2$) and radicals ($SO_5^{\bullet-}$ and $SO_4^{\bullet-}$) were involved in the reaction process and the $SO_5^{\bullet-}$ generated by the oxidation of PMS played a crucial role in the TCH degradation. The possible reaction mechanism was finally proposed. This study provided new insight into the Z-scheme heterostructure to promote the photo-assisted Fenton-like reaction.

The photo-assisted Fenton-like reaction with peroxymonosulfate (PMS) as the oxidant has attracted great attention for rapid treatment of aqueous emerging pollutants [1–3]. The introduction of PMS can regulate the introduction of the long-lived $SO_4^{\bullet-}$ free radical, and increase the content of other reactive oxygen species (ROS) in the system [4,5]. Meanwhile, the introduced PMS captures the photogenerated electron-hole pairs to be activated, so that the exciton recombination rate is reduced and the light utilization efficiency is improved [6].

Previous reports have confirmed that the PMS could be effectively activated by transition metal-based photocatalysis, where $NiCo_2O_4$ has been regarded as the promising catalyst due to its narrow band gap and bimetallic active centers [7]. Nonetheless, severe leaching of transition metal ions and short photo-generated carrier lifetime of $NiCo_2O_4$ hinder its potential of application. It was documented that constructing heterostructure by introduction of energy-level matched co-catalyst $Bi_{24}O_{31}Br_{10}$ could be an effective solution [8]. However, as a type-II heterojunction, the reported $NiCo_2O_4/Bi_{24}O_{31}Br_{10}$ (NB) could not make full use of highly active photo-generated carriers, resulting in its inability to efficiently activate PMS with insufficient pollutant removal efficiency. The Z-scheme heterostructure strategy can effectively inhibit the recombination of photogenerated carriers and retain the high-level redox potential, thereby better promoting the synergistic effect of photocatalysis and PMS activation [6]. Inserting suitable materials as electronic "ladder" between $NiCo_2O_4$ and $Bi_{24}O_{31}Br_{10}$ may realize the construction of Z-scheme heterojunction. The wide band gap semiconductor BiOCl, with the conduction band position at about −0.1 eV, could act as a candidate for the introduced semiconductor [9,10]. Simultaneously, relying on the open layered crystal structure of $Bi_{24}O_{31}Br_{10}$, providing sufficient Cl ions in the hydrothermal system may bring about the in-situ generation of BiOCl on the surface

* Corresponding author.
E-mail address: dongshuangshi@gmail.com (S. Dong).
[1] These authors contributed equally to this work.

https://doi.org/10.1016/j.cclet.2022.05.017
1001-8417/

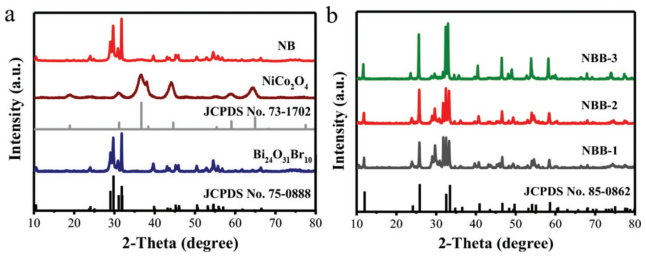

Fig. 1. (a, b) The XRD patterns of as-prepared catalysts.

of $Bi_{24}O_{31}Br_{10}$ [11]. Therefore, selecting suitable precursor materials can achieve the simultaneous synthesis of BiOCl and $NiCo_2O_4$.

Based on the above, this study constructed a $NiCo_2O_4$/BiOCl/$Bi_{24}O_{31}Br_{10}$ (NBB) ternary Z-scheme heterojunction, which was marked as NBB-1, NBB-2 and NBB-3 according to the concentration of $NiCl_2$ and $CoCl_2$ in the precursor from low to high, and the synthesis process details were shown in Supporting information. The properties and degradation performance of the composite catalyst were explored, and the catalytic reaction mechanism under vis/PMS was finally determined.

The composition and structure information of the catalysts could be obtained by XRD patterns (Fig. 1). The peaks symbolizing $Bi_{24}O_{31}Br_{10}$ (JCPDS No. 75–0888) and BiOCl (JCPDS No. 85–0862) were evidently shown in the curves of the as-prepared NBB catalysts [12,13]. This indicated that the Cl element introduced in the composite materials was in the form of BiOCl crystals, meanwhile, BiOCl would appear as the main phase (NBB-3) when the amount of Cl introduced was high (molar ratio of Cl^-/$Bi_{24}O_{31}Br_{10}$ at 2.80). The characteristic peaks of $NiCo_2O_4$ could not be clearly observed in the XRD pattern of the NBB catalysts, which was mainly due to the poor crystallization performance of $NiCo_2O_4$. In addition, the diffraction peak of each control sample was highly consistent with its corresponding standard card, and there was no obvious impurity peak in all XRD patterns, indicating that the synthesized samples were all high in purity and free of other impurities. The morphology structure, elemental distribution and surface functional groups of the catalysts were examined by SEM, TEM, STEM-EDX elemental mapping and FI-IR (Figs. S1 and S2 in Supporting information). All the results confirmed the successful synthesis of $NiCo_2O_4$/BiOCl/$Bi_{24}O_{31}Br_{10}$. Combined with the XRD characterization results, the synthesis reaction process of the NBB catalysts was speculated as follows. During the hydrothermal synthesis of the composite material, the Cl^- in the reaction system penetrated into the $Bi_{24}O_{31}Br_{10}$ surface structure and replaced some of the Br sites. Then, the surface lattice of $Bi_{24}O_{31}Br_{10}$ collapsed due to the excessive amount of Cl^- substitution, thereby forming BiOCl/$Bi_{24}O_{31}Br_{10}$ with a similar core-shell structure. Finally, $NiCo_2O_4$ was successfully synthesized and attached to the surface of BiOCl/$Bi_{24}O_{31}Br_{10}$ to form $NiCo_2O_4$/BiOCl/$Bi_{24}O_{31}Br_{10}$ (NBB).

The element composition in the NBB-2 catalyst were obtained by XPS analysis. As shown in the survey spectrum (Fig. S3 in Supporting information), the composite mainly contained seven elements: Co, Ni, O, Bi, Cl and Br. The Bi 4f XPS spectrum of the catalyst (Fig. 2a) showed that the NBB material had two obvious peaks at 158.6 and 163.9 eV, matching to Bi $4f_{5/2}$ and Bi $4f_{7/2}$ in Bi^{3+}, respectively [14]. The O 1s (Fig. 2b) could be deconvoluted into four peaks located at 529.2, 529.8, 531 and 532.3 eV, representing lattice oxygen, Br–O bond, Cl–O bond and O–H bond in water molecules adsorbed on the catalyst surface, respectively [15]. The high-resolution XPS of Br 3d and Cl 2p were further presented in Figs. 2c and d. The diffraction peaks at 67.7 and 68.3 eV corresponded to Br $3d_{3/2}$ and Br $3d_{5/2}$, while the peaks at 197.8 and 199.1 eV matched up with Cl $2p_{3/2}$ and Cl $2p_{1/2}$ [16,17]. For Co 2p (Fig. 2e), the Co $2p_{3/2}$ and Co $2p_{1/2}$ diffraction peaks could both be deconvoluted into two small peaks separately symbolizing Co^{2+} (780.1 and 795.3 eV) and Co^{3+} (797.1 and 781.9 eV) [18]. Similarly, the diffraction peaks at 855.1 and 873.3 eV attributed to Ni^{2+} and the peaks at 856.7 and 875.1 eV corresponding to Ni^{3+} could be observed in Fig. 2f [18]. The multivalent state of metal elements was beneficial to promote the activation of PMS. Simultaneously, XPS characterization results further confirmed the composite coexistence of $NiCo_2O_4$, BiOCl and $Bi_{24}O_{31}Br_{24}$ in NBB-2.

Tetracycline hydrochloride (TCH) degradation experiments were performed to investigate the efficacy of the nascent catalysts and the results were shown in Fig. 3a. The order of TCH removal efficiencies in 2 min was observed as NBB-2 > NBB-3 > NBB-1 > NB > $Bi_{24}O_{31}Br_{10}$ > $NiCo_2O_4$ which was also consistent with the mineralization performance of catalysts (Fig. S4 in Supporting information). The corresponding rate constants of the first-order reaction kinetics fitting were given in Table S2 (Supporting information). NBB-2 exhibited the highest catalytic performance with its reaction kinetic rate constant of 0.8481 min^{-1} much higher than those in the same reaction system reported in recent years (Table S3 in Supporting information). According to the apparent property of the degradation curve, the catalytic reaction process could be divided into two stages with 0.5 min as the boundary. The composite catalysts all possessed relatively high degradation rate in the first 0.5 min, and then significantly decreased. Similar phenomena have also been reported in some research of Co-based compound semiconductor materials [7,19]. This was owing to the strong effect of Co(II) on the O–O bond in PMS molecule to produce abundant ROS, and the construction of heterojunction could effectively accelerate the Co(III)/Co(II) redox cycle [20]. The degradation rate constant of NBB-2 in the first stage was also the greatest (2.0232 min^{-1}), indicating the successful construction of the ternary heterojunction.

Fig. 3b displayed the degradation of TCH in different reaction systems. The results illustrated that the introduction of visible light, PMS or catalyst alone had almost no effect on the degradation of TCH. Compared with single photocatalysis and Fenton-like systems, the catalytic performance of the photo-assisted Fenton-like composite system was significantly enhanced. For further clarifying the reaction mechanism of photocatalyst activation PMS, a synergy factor (S) was introduced with reference to the similar study, and the calculation was carried out according to Eq. 1 [21]:

$$S = \frac{k_{vp}}{k_v + k_p} \quad (1)$$

where k_{vp}, k_v and k_p correspond to the kinetic constants of the NBB-2/vis/PMS, NBB-2/vis and NBB-2/PMS systems, respectively, and they were given in Table S2. The S value was calculated to be 1.43, greater than 1, indicating that the photocatalytic reaction and Fenton-like reaction in the composite reaction system did not exist independently but were promoted synergistically. Furthermore, the S value of the NB/vis/PMS system in the previous study was calculated according to this method to be 1.11, which is significantly smaller than that of the NBB-2/vis/PMS system, confirming that the introduced BiOCl is beneficial to promote the coupling of photocatalysis and PMS activation [8]. In the catalyst/vis/PMS composite system, the holes and electrons excited by visible light accelerated the PMS activation process, and simultaneously reduced the recombination of electron-hole pairs. The effect of various operating parameters on degradation efficiency were explored and the relating results were displayed in Fig. S5 (Supporting information). The results of catalyst recycling and ion leaching tests verified that the as-prepared NBB-2 possessed good chemical stability and reusability (Figs. S6–S8 in Supporting information).

The free radical scavenger experiments and ESR test were carried out to determine the reactive species in the vis/PMS system.

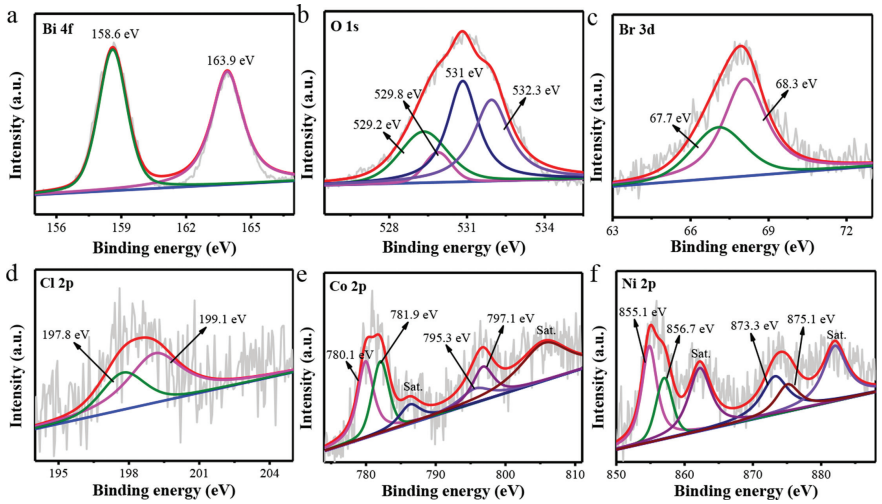

Fig. 2. High-resolution XPS of Bi 4f (a), O 1s (b), Br 3d (c), Cl 2p (d), Co 2p (e) and Ni 2p (f), respectively.

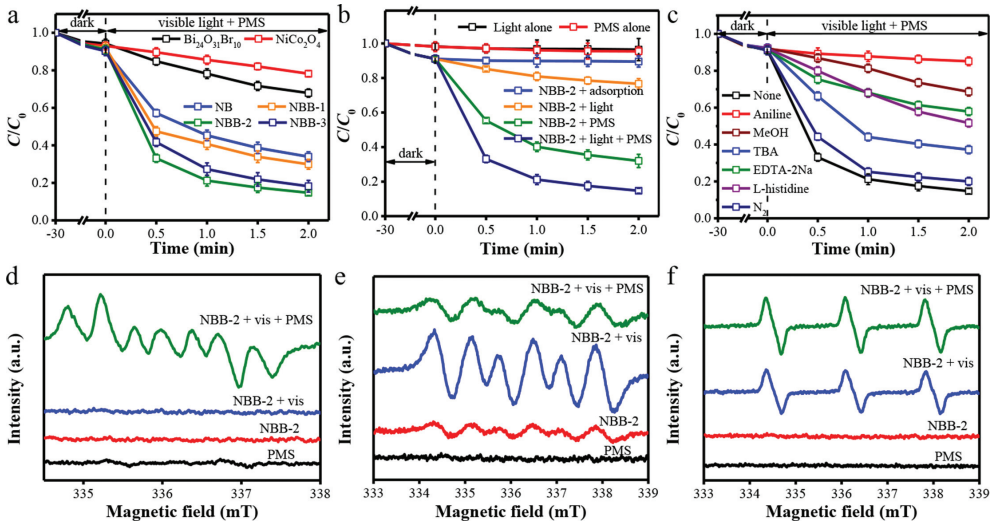

Fig. 3. (a) TCH degradation performance of the synthesized samples under PMS/vis system. (b) The effect of reaction protocols of TCH on NBB-2 performance. (c) Free radical scavenger experiments with NBB-2 in vis/PMS system. ESR spectra in different systems: (d) $^{\bullet}OH$ and $SO_4^{\bullet-}$-DMPO in water, (e) $^{\bullet}O_2^-$-DMPO in methanol, and (f) $^1O_2$-TEMP in water.

The results demonstrated that $SO_5^{\bullet-}$, $SO_4^{\bullet-}$, holes and $^1O_2$ played a significant role in the reaction process, and $^{\bullet}OH$ and $^{\bullet}O_2^-$ also participated in the reaction (Fig. 3c). Figs. 3d-f are the ESR detection spectra of $SO_4^{\bullet-}$, $^{\bullet}OH$, $^{\bullet}O_2^-$ and $^1O_2$, respectively. It could be observed in Fig. 3d that the signals of $SO_4^{\bullet-}$ and $^{\bullet}OH$ were only existing in the catalyst/vis/PMS system. This is consistent with the material properties. In the catalyst/vis system, the valence band (VB) energy of $NiCo_2O_4$ and $Bi_{24}O_{31}Br_{10}$ was too low to produce $^{\bullet}OH$, and BiOCl with a higher valence band position could not be excited by visible light on account of its wide band gap [8,10]. For $^{\bullet}O_2^-$ (Fig. 3e), the weak ESR signal was shown under the condition of only catalyst, suggesting that the catalyst itself could activate the dissolved oxygen in the solution. After the introduction of visible light, $^{\bullet}O_2^-$ signal intensity increased significantly, indicating that the photoexcited carriers were retained in the conduction band (CB) of $NiCo_2O_4$ with higher energy instead of being transferred to the CB of BiOCl, which could not produce $^{\bullet}O_2^-$. This result convinced the successful construction of the Z-scheme heterojunction. After further adding PMS, it might promote the conversion of $^{\bullet}O_2^-$ into other free radicals such as $^1O_2$, resulting in weakening of the ESR signal intensity, which also confirmed the results of the masking experiment. As shown in Fig. 3f, there was no $^1O_2$ produced in the case of only PMS and only catalyst. The $^1O_2$ signal of the photo-assisted Fenton-like system was stronger than that of the photocatalytic system, because the introduction of PMS might provide more $^1O_2$ generation pathways [22]. The ESR results verified the existence of $SO_4^{\bullet-}$, $^{\bullet}OH$, $^{\bullet}O_2^-$ and $^1O_2$ in the reaction system, and confirmed the superiority of the photo-assisted Fenton-like system.

The UV–vis diffuse reflection spectra of the as-prepared catalysts were displayed in Fig. 4a. It could be observed that $NiCo_2O_4$ had a full-spectrum absorption capacity, while the light absorption boundary of $Bi_{24}O_{31}Br_{10}$ was 467 nm. Compared with the pure $Bi_{24}O_{31}Br_{10}$, the absorption intensity of the NB composite catalyst had also been significantly improved. Suggesting that the formation of the $NiCo_2O_4/Bi_{24}O_{31}Br_{10}$ heterojunction could increase the visible light absorption capacity of the catalyst [23]. After the introduction of BiOCl, the absorption range and intensity of NBB-2 were also enlarged compared to NB, which further illustrated that the Z-scheme heterojunction had a better light utilization capability than the type-II heterojunction.

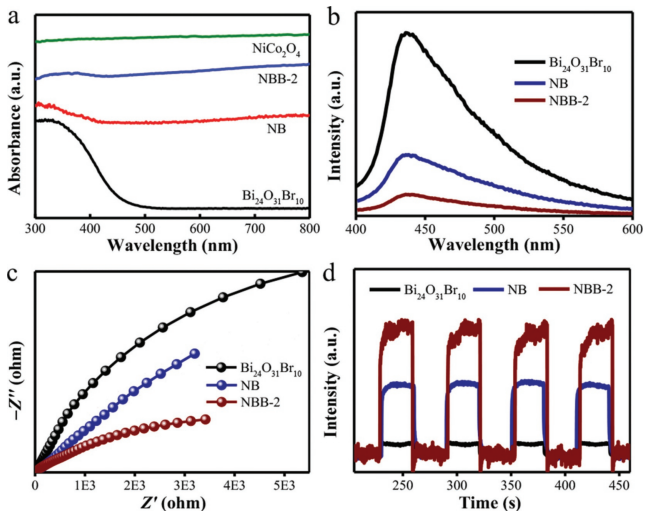

Fig. 4. (a) UV–vis DRS of as-prepared samples. (b) PL, (c) EIS Nyquist plots and (d) photocurrent of pristine $Bi_{24}O_{31}Br_{10}$, NB and NBB-2.

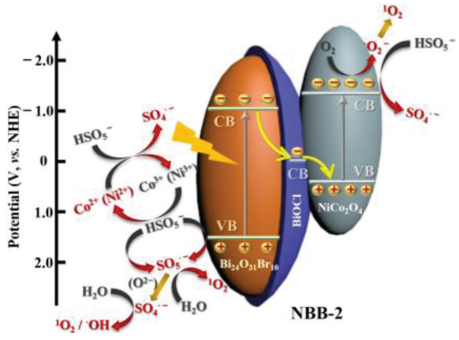

Fig. 5. Schematic degradation mechanism for as-prepared catalysts in vis/PMS system.

The separation efficiency of electron-hole pairs and the carrier transport ability were intently related to the catalytic performance of the material, thus, photoluminescence spectroscopy (PL), electrochemical impedance spectra (EIS) and transient photocurrent (Figs. 4b-d) were characterized. Compared with $Bi_{24}O_{31}Br_{10}$ and NB composites, the PL intensity of NBB-2 was significantly reduced, indicating that the Z-scheme heterojunction could better inhibit exciton recombination [24,25]. EIS Nyquist spectrum showed that NBB-2 exhibited the smallest arc radius, manifesting that it possessed the best electron-hole pair separation and carrier transport ability [26,27]. At the same time, NBB-2 had the highest photocurrent density under visible light, demonstrating that the introduction of BiOCl significantly promoted the effective utilization of photogenerated carriers [28,29]. The photoelectric characterization of the catalyst all confirmed the successful construction of the Z-scheme heterostructure.

Based on the previous results, the possible mechanism of PMS activation by NBB-2 was illustrated in Fig. 5. Different from the type-II heterostructure of the binary composite NB, the BiOCl introduced in NBB-2 presented as a "ladder" for electron transfer to construct a Z-scheme heterostructure. The band gap and conduction/valence band position of $Bi_{24}O_{31}Br_{10}$ and $NiCo_2O_4$ prepared by hydrothermal method had been determined in the previous work of our research group, and the relevant data were given in Table S4 (Supporting information). Under visible light irradiation, $Bi_{24}O_{31}Br_{10}$ and $NiCo_2O_4$ were excited, while BiOCl could not be excited due to its wide band gap (~3.3 eV). The photogenerated electrons in the CB of $Bi_{24}O_{31}Br_{10}$ combined with the photogenerated holes in the VB of $NiCo_2O_4$ through the CB of BiOCl, and the high-energy electrons and holes were retained. This process was consistent with the ESR test results. Then, the electrons/holes of NBB-2 respectively underwent reduction/oxidation reactions with the PMS to form $SO_4^{\bullet-}$/$SO_5^{\bullet-}$. Simultaneously, $^{\bullet}O_2^-$ formed by O_2 capturing photogenerated electrons could also reduce HSO_5^- to generate $SO_4^{\bullet-}$ and $^1O_2$ [30]. It is worth noting that, according to the results of the free radical trapping experiment, the oxidation reaction occurring in the VB should be dominant. The carrier trapping reaction of PMS at the energy band of the catalyst could effectively reduce the recombination of electron-hole pairs and improve the utilization of photogenerated carriers. At the same time, the high-energy position of energy band of the Z-scheme heterojunction also enabled the feasibility of PMS activation reaction occurring. The transition metals in the composite material also participated in the PMS activation through gain and loss of electrons [26,31]. The highly active $SO_5^{\bullet-}$ could be converted into $SO_4^{\bullet-}$ (and $^1O_2$), and $SO_4^{\bullet-}$ could also be further reacted to obtain $^{\bullet}OH$ and $^1O_2$ [32].

In summary, this study successfully constructed ternary composite catalyst with a Z-scheme heterostructure, and studied its catalytic degradation performance of pollutant in the photo-assisted Fenton-like system. The selected NBB-2 ($NiCo_2O_4$/BiOCl/$Bi_{24}O_{31}Br_{10}$) exhibited high TCH degradation efficiency, stable property, and reusability. Correspondingly, the mechanism of the photo-assisted Fenton-like system had also been explored. In the composite reaction system, the effects of visible light and PMS were mutually reinforcing, rather than independent. The activation process of PMS in the system was mainly owing to the oxidation by photo-generated holes and high-valence transition metals. The generated $SO_5^{\bullet-}$ had high reactivity and could further generate other free radicals to remove pollutants. This work proposed a new reaction path for the photo-assisted Fenton-like reaction system.

Declaration of competing interest

The authors declare that they have no known competing financial interests or personal relationships that could have appeared to influence the work reported in this paper.

Acknowledgments

This work was financially supported by the National Natural Science Foundation of China (Nos. 52170079 and U20A20322) and the Programme of Introducing Talents of Discipline to Universities, China (No. B16020).

Supplementary materials

Supplementary material associated with this article can be found, in the online version, at doi:10.1016/j.cclet.2022.05.017.

References

[1] J.J. Qi, J.Z. Liu, F.B. Sun, et al., Chin. Chem. Lett. 32 (2021) 1814–1818.
[2] X.M. Hao, G.L. Wang, S. Chen, H.T. Yu, X. Quan, Front. Environ. Sci. Eng. 13 (2019) 77.
[3] M. Zhu, L.S. Zhang, S.S. Liu, et al., Chin. Chem. Lett. 31 (2020) 1961–1965.
[4] L.S. Zhang, X.H. Jiang, Z.A. Zhong, et al., Angew. Chem. Int. Ed. 60 (2021) 21751–21755.
[5] C. Lyu, L. Zhang, D. He, B.Y. Su, Y. Lyu, Chin. Chem. Lett. 33 (2022) 930–934.
[6] J.J. Jiang, X.Y. Wang, C.L. Yue, et al., J. Hazard. Mater. 414 (2021) 125528.
[7] M.J. Xu, H.Y. Zhou, Z.L. Wu, et al., J. Hazard. Mater. 399 (2020) 123103.
[8] Y.Y. Song, J.J. Jiang, Y.H. Ma, T.R. Li, S.S. Dong, Catal. Sci. Technol. 11 (2021) 2110–2118.
[9] F.Y. Du, Z. Lai, H.Y. Tang, H.Y. Wang, C.X. Zhao, Chemosphere 287 (2022) 132391.
[10] H.F. Cheng, B.B. Huang, Y. Dai, Nanoscale 6 (2014) 2009–2026.
[11] X. Chen, J. Zhang, L. Liu, et al., Appl. Surf. Sci. 491 (2019) 1–8.

[12] R. Li, J.Q. Feng, X.C. Zhang, et al., Sep. Purif. Technol. 247 (2020) 117007.
[13] Z.X. Yang, Z.C. Shang, F. Liu, et al., Nanotechnology 32 (2021) 205602.
[14] J. Bai, X. Wang, G. Han, et al., J. Alloys Compd. 859 (2021) 157837.
[15] S. Heidari, M. Haghighi, M. Shabani, J. Clean. Prod. 259 (2020) 120679.
[16] X.K. Sun, C.G. Li, Q.Y. Zhu, et al., Anal. Chim. Acta 1140 (2020) 122–131.
[17] R.Y. Zhang, S.Y. Niu, J.M. Xiang, et al., Sep. Purif. Technol. 261 (2021) 118258.
[18] J.C. Liu, Z.H. Yang, L.J. Yang, et al., J. Alloys Compd. 853 (2021) 157403.
[19] X.Y. Wang, J.J. Jiang, Y.H. Ma, et al., J. Colloid Interface Sci. 600 (2021) 449–462.
[20] Q.T. Sun, B.D. Xu, J. Yang, T.T. Qian, H. Jiang, Chem. Eng. J. 400 (2020) 125899.
[21] P.P. Qiu, T. Zhao, X.H. Zhu, et al., Chin. Chem. Lett. 32 (2021) 1456–1461.
[22] Y.J. Li, J. Li, Y.T. Pan, et al., Chem. Eng. J. 384 (2020) 123361.
[23] X.H. Jiang, L.S. Zhang, H.Y. Liu, et al., Angew. Chem. Int. Ed. 59 (2020) 23112–23116.
[24] J. Zhang, D.D. Zhou, S.S. Dong, N.Q. Ren, J. Hazard. Mater. 366 (2019) 311–320.
[25] X.H. Jiang, F. Yu, D.S. Wu, et al., Chin. Chem. Lett. 32 (2021) 2782–2786.
[26] F.H. Mu, B.L. Dai, W. Zhao, et al., Chin. Chem. Lett. 32 (2021) 2539–2543.
[27] F. Yu, L.C. Wang, Q.J. Xing, et al., Chin. Chem. Lett. 31 (2020) 1648–1653.
[28] Y. Kim, E. Coy, H. Kim, et al., Appl. Catal. B 280 (2021) 119423.
[29] J.P. Zou, D.D. Wu, J.M. Luo, et al., ACS Catal. 6 (2016) 6861–6867.
[30] J.J. Jiang, X.Y. Wang, C.J. Zhang, et al., Chem. Eng. J. 397 (2020) 125356.
[31] L. Liu, Y.N. Li, W. Li, et al., Environ. Res. 187 (2020) 109665.
[32] X.X. Long, C.P. Feng, D.H. Ding, et al., J. Hazard. Mater. 418 (2021) 126357.